Spin-Relaxation Dynamics of E^{′} Centers at High Density in SiO_{2} Thin Films for Single-Spin Tunneling Force Microscopy

K. Ambal, A. Payne, D. P. Waters, C. C. Williams, and C. Boehme

Phys. Rev. Applied **4**, 024008 — Published 17 August 2015

DOI: 10.1103/PhysRevApplied.4.024008

E'-center spin dynamics in silicon dioxide thin films with high E'-center densities for single spin-tunneling force microscopy

K. Ambal, A. Payne, D. P. Waters, C.C. Williams,* and C. Boehme†
Department of Physics and Astronomy, University of Utah, Salt Lake City, UT 84112

The suitability of the spin–dynamics of paramagnetic silicon dangling bonds (E' centers) in high E'-density amorphous silicon dioxide (SiO_2) as probe spins for single–spin tunneling force microscopy (SSTFM) is studied. SSTFM is a spin–selection rule based scanning–probe single–spin readout concept. Following the synthesis of SiO_2 thin films on (111) oriented crystalline silicon substrates with room–temperature stable densities of $[E'] > 5\times10^{18}cm^{-3}$ throughout the 60nm thin film, pulsed electron paramagnetic resonance spectroscopy was conducted on the E' centers at temperatures between $T = 5K$ and $T = 70K$. The measurements revealed that the spin coherence (the transverse spin-relaxation time T_2) of these centers is significantly shortened compared to low-E' density SiO_2 films and within error margins not dependent on temperature. In contrast, the spin–flip times (the longitudinal relaxation times T_1) are dependent on the temperature but with much weaker dependence than low–density SiO_2, with greatest deviations from low–density SiO_2 seen for $T = 5K$. These results, discussed in the context of the spin–relaxation dynamics of dangling bond states of other silicon–based disordered solids, indicate the suitability of E' centers in high-density SiO_2 as probe spins for SSTFM.

PACS numbers: 76.30.-v, 77.84.Bw, 03.67.-a, 68.37.Ef

I. INTRODUCTION

Over the past two decades, the promise of quantum information applications based on localized paramagnetic states has been one of the driving forces behind the rapid development of various and single-spin detection and readout schemes [1–4]. Experimentally demonstrated readout schemes differ conceptually significantly. Most utilize various spin–to–charge or spin–to–optical photon transition mechanisms in order to convert the weak interaction energies of electron and nuclear spins into straight forwardly detectable observables (by means of charge [4] or photon detection [1]). Other spin–detection schemes are based on scanning probe microscopy [2, 5]. For instance, magnetic resonance force microscopy is capable of directly measuring the minute magnetic force produced by a single spin. This however, is only possible with limited spatial resolution (nm scales rather then atomic scales) and long measurement times [6] or they require sufficiently conductive probes or substrates [7, 8] whose charge carrier reservoirs can be detrimental for the coherence times of localized spin–qubits.

We have therefore described recently [9] a force detected scanning probe based single spin–readout that combines the advantages of high spatial resolution with the advantage of using spin–selection rules for the conversion of spin–states into straight forwardly detectable charge states. An illustration of this concept is shown in Fig. 1(a). It consists of a low–magnetic field magnetic resonance setup combined with a scanning force probe whose tip consists of a dielectric material with a highly localized paramagnetic electron state, the so–called probe spin, right at the apex. The idea behind this concept is to utilize scanning probe force microscopy for the detection of individual charge transitions and to then detect spin states through spin–selection rules that control these charge transitions [10, 11]. By adjustment of the electronic energy levels of probe spin and test spin, spin–dependent tunneling causes electrostatically induced force noise which reveals the spin dynamics of the test/probe spin pair [9]. The contrast of this single spin–tunneling force microscope (SSTFM) detection approach to existing force–microscopy based spin–detection schemes is that those are based on the direct detection of very weak dipolar magnetic forces [2] or combinations of spin–selection rule governed optical transitions with scanning probe techniques [6], while SSTFM relies on the measurement of Coulomb–forces which are many orders of magnitude stronger. We note that for the presence of pronounced spin–selection rules, weak spin–orbit coupling is needed in order to oppress spin–orbit transitions. This is the case for instance in silicon based materials (mono-, poly, micro-, and nano-crystalline as well as amorphous silicon, silicondioxde, siliconnitride combinations thereof) where many spin–dependent transitions between localized paramagnetic states are known [10–13].

For the implementation of SSTFM, Payne et al. [9] suggested to use a crystalline silicon (c-Si) scanning probe tip with an amorphous silicondioxide (SiO_2) film in which a single E' center [14–17] would be used as probe spin, located at the apex. E' centers exhibit positive correlation energies and are therefore paramagnetic, a property that allows them to be studied with electron paramagnetic resonance (EPR) spectroscopy [18, 19]. As E' centers have been studied extensively with regard to their behavior as trap states in SiO_2–based electronic devices (e.g. the gate dielectric of silicon thin film transistors [15]), most

* clayton@physics.utah.edu
† boehme@physics.utah.edu

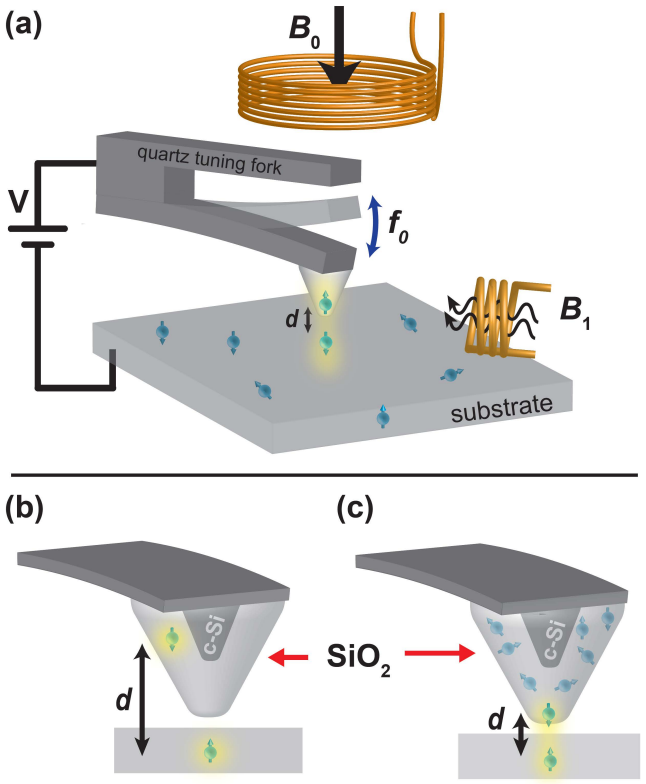

FIG. 1. (a) Illustration of the SSTFM concept as outlined in detail by Payne et al. [9]. The setup includes mutually perpendicular coils that allow the generation of static and an oscillating magnetic fields B_0 and B_1, respectively for low–magnetic field magnetic resonance and a force detector with a dielectric tip that has a highly localized probe spin close to its apex. Payne et al. have proposed SiO_2 as dielectric tip material and the E' center therein as probe spin. (b) and (c) illustrate that the density of the randomly generated E' centers in the amorphous SiO_2 layer must be high enough such that an E' center is likely to be located within a minimal distance d of the tip apex such that enough exchange between probe spin and test spins can be established by tip positioning such that significant spin–dependent tunneling rates are possible.

studies of E' center properties in the past have focused primarily on how E' center densities can be minimized by SiO_2 preparation and treatment. Few studies have focused on the dynamic properties of this spin $s = 1/2$ system, but those that have show that E' centers exhibit remarkably long longitudinal (T_1) spin relaxation times over large temperature ranges [17, 20–23]. At room temperature, T_1 times on the order of hundreds of microseconds have been reported [22]. This is long compared to the T_1 times of silicon dangling bonds at the SiO_2 to crystalline silicon (c-Si) interface [12] (the so called P_b centers) and it is comparable to other bulk silicon dangling bond states, e.g. in amorphous silicon [24] or microcrystalline silicon [25, 26].

Since E' centers develop at random sites within the continuous random network of SiO_2, Payne et al. [9] suggested to obtain an individual probe spin within a few Ångstroms of the tip apex by growth of an SiO_2 layer on a c-Si cantilever with high enough density [E'] of E' centers such that a sufficiently large probability exists that a single E' center is close enough to the apex. An appropriate proximity would be defined by a distance d such that significant tunneling probability to a localized state outside of the tip material is possible [see illustration in Fig. 1(b) and (c)]. Thus, [E'] must be high enough such that the probability to find an E' center within appropriate apex vicinity is within the order of unity. For this density, the E' centers must be chemically and optically stable over long time scales (weeks or months), preferably at room temperature. Furthermore, E' centers in such high-[E'] SiO_2 must exhibit similarly long transverse spin relaxation times (T_1) as E' centers in low–[E'] SiO_2. If the mutual proximity of the E' states significantly increases spin relaxation rates, applicability for spin readout will be limited [9].

In the following sections, we present measurements of the spin–relaxation dynamics of E' centers for high-[E'] films. Both, T_1 and T_2 are studied after we first describe the synthesis of SiO_2 thin films with highest thermally and optically stable densities of E' centers. The results of this study will then be discussed with regard to the suitability of the created high–[E'] SiO_2 for SSTFM.

II. EXPERIMENTAL TECHNIQUES

For the corroboration of E' center densities as well as the measurements of spin–relaxation times, continuous wave (cw) EPR [18] and pulsed (p) EPR experiments [19] were carried out, respectively. The experiments were conducted at X-band frequencies using a cylindrical dielectric resonator as part of a Bruker Flexline EPR probehead, a Bruker Elexsys E580 EPR spectrometer, and an Oxford flow cryostat for the temperature adjustment. The cw EPR experiments were conducted using a lock–in detected modulation of the quasi–static magnetic field B_0 with an amplitude of ≈ 0.1mT and a frequency of 10KHz. The quasi static field B_0 was then adiabatically swept in order to find the EPR resonance condition where the Zeeman splitting of the paramagnetic centers is tuned to the applied microwave radiation.

For each cw EPR measurement, the sample was inserted into the dielectric resonator and the resonator was critically coupled to the microwave circuit. Because of the field modulated lock–in detection, all cw EPR absorption spectra display the first derivative of the real absorption function. Integrating lock–in detected absorption spectra produces the real EPR absorption spectra and the areas under these functions are proportional to the number of paramagnetic centers that in the observed EPR line. For the absolute quantification of the density of paramagnetic states that belong to an observed resonance line, the line integral is scaled by a reference line integral that stems from the spectrally well–separated

phosphorous (^{31}P) donor resonance that is caused by the well–known donor bulk density in the crystalline silicon sample substrate as outlined in detail below.

For the pEPR experiments, the dielectric resonator was decoupled in order to increase its band width. For the measurements brief ($\sim$ 16ns) high–power (up to 1kW) microwave pulses or pulse sequences were irradiated under resonant condition. The radiation response of the sample was then detected using solid state detection diodes and recorded using a Bruker Specjet transient recorder. For the determination of the longitudinal and transverse spin–relaxation times T_1 and T_2, an inversion–recovery sequence and a standard two–pulse Hahn–echo sequence were used, respectively, as described in the literature [19].

III. MATERIALS PREPARATION: SYNTHESIS OF THIN SiO_2 FILMS WITH VERY HIGH E' CENTER DENSITIES

An estimate for the active tip volume in which a single E' center can be utilized as a probe spin for SSTFM in the grown oxide layer can be obtained from the product of a typical tip surface area of less than 300nm^2 for a 25nm tip radius and a typical tunneling depth of less than 2nm [9]. Thus, [E′] $\approx 10^{18}$cm^{-3} to 10^{19}cm^{-3} is needed. This is higher than the highest previously reported values for [E'] [15] which were generated via electric currents through SiO_2 gate dielectrics, a procedure that is hardly applicable to cantilever surfaces. These unprecedented high values for [E'] needed for the proposed spin–readout concept raise the question if continuous random SiO_2 networks can even exits under these conditions or whether quick recombination of E' centers into silicon–silicon bonds will put an upper limit on [E'].

Theoretical calculations do not prohibit the existence of such SiO_2 layers: Constraint Theory [27] applied to thin SiO_2 layers only imposes lower limits on silicon dangling bond densities in both the bulk (the E' states) as well as the crystalline silicon to SiO_2 interface [28] (where silicon bonds are called P_b centers), predominantly due to the flexibility of the wide range of the oxygen bond–angles. Furthermore, due to the bond length constraint in the lower Å–range, recombination of adjacent E' states into Si–Si bonds is not expected either for [E′] $\leq 10^{19}$cm^{-3}. However, under the assumption of dangling bond distances below 5nm ([E′] $\sim 10^{19}$cm^{-3}), the continuous random network is expected to be significantly underconstrained causing the resulting network to soften to a degree where local network elements will undergo localized motion (through wagging, streching, and rocking transitions) that departs entirely from the phonon mode structure of low-[E'] SiO_2.

For the study of various E' preparation techniques that can induced very high [E'], we used n-type, ^{31}P doped ([^{31}P]$\approx 10^{15}$cm^{-3}) Czochralski grown c-Si(111) wafers. The use of ^{31}P doped material allowed a very accurate determination of the E' densities from EPR spectra since the well known hyperfine split ^{31}P resonance could be used as an in-sample spin-standard. The 300 micrometer thick 3" wafers were first annealed in oxygen at atmospheric pressure and 1000°C in order to form an approximately 60nm thick (profilometer measured) thermally grown SiO_2 layer. The oxidized samples were then diced into 60mm x 3mm size EPR compatible rectangles. The black data points of Fig. 2 display an EPR spectrum of the as prepared thermal oxides. The two peaks are due to the hyperfine split ^{31}P resonance that, due to the known ^{31}P bulk density and therefore areal density ($\approx 3\times10^{13}$cm^{-2}), can be used to calibrate the magnetic field and density scales for the E' center measurements. The black data points show almost no resonant features next to the ^{31}P hyperfine peaks which means that E' densities in as grown samples are below the detection limit which is $\approx 1\times10^{12}$cm^{-2} for the given measurement conditions. This corresponds to an average volume density below $\approx 1.67\times10^{17}$cm^{-3} within the 60nm thin film. Thus, given that previous reports of E' densities in thermally grown SiO_2 are all significantly below the 10^{17}cm^{-3} limit, we expected no significantly different EPR signals from E' centers for the as grown oxide layers.

In order to explore how to create E' densities $> 10^{17}$cm^{-3}, the thin SiO_2 layer was exposed to (i) ultraviolet (UV) radiation [29] (produced by a NdYAG laser with 264nm wave length) for six hours, (ii) gamma radiation produced by a ^{137}Cs sample for 24 hours, producing an overall irradiation dose of about 10-12Mrad [30], (iii) different growth temperatures during the thermal growth, (iv) an Ar-ion discharge plasma excited by a 300W 13.56MHz RF excitation at 0.5sccm gas flow and a pressure of 10mTorr [31, 32]. We then conducted EPR measurements similar to those shown in Fig. 2 on the samples treated according to (i), (ii), and (iii). These measurements revealed similar results compared to the as grown sample, represented by the black data in Fig. 2. This again confirmed the previous reports that treatment of SiO_2 layers following these methods may increase the E' center densities but not beyond the 10^{17}cm^{-3} range.

In contrast, the application of the Ar-ion plasma treatment (method iv) caused a significant increase of the E' density, as indicated by the blue circled data points in Fig. 2. The plot displays a feature at a magnetic field of approximately 348mT, corresponding to a Landé-factor of $g \approx 2.001$ which is attributed to plasma induced E' centers. The average E' center volume density in this film derived from the measured areal density per film thickness is 6×10^{18}cm^{-3}, determined by using the ^{31}P donor spins in the silicon substrate as a reference. While this observation shows that the plasma exposure of the oxide film is able to generate a large quantity of paramagnetic species at the g-factor anticipated for E' centers, it is not clear whether these states are all E' centers (silicon dangling bonds within the SiO_2 bulk). Other paramagnetic species such as interface defects between the SiO_2 layer and the c-Si bulk (if the etch has not removed the entire

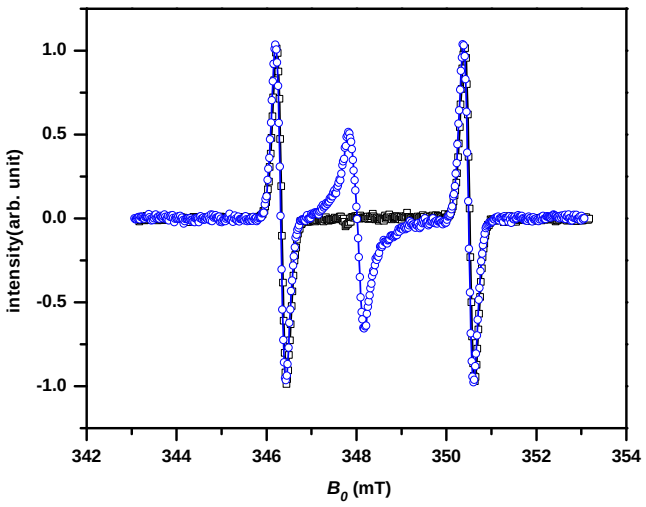

FIG. 2. Plots of X-Band EPR spectra of 60mm x 3mm x 0.3mm large ^{31}P doped c-Si(111) samples measured at a temperature $T = 20$K with a field modulation frequency $f = 10$kHz, a modulation amplitude of 0.1mT, and a weak microwave power of 4μW to avoid saturation. The samples had 60nm thin layers of thermally grown SiO_2. The black data points represent measurements of the as prepared thermal oxide. The blue data points show a measurements under identical conditions after the sample was been exposed to an argon ion plasma for 5 minutes.

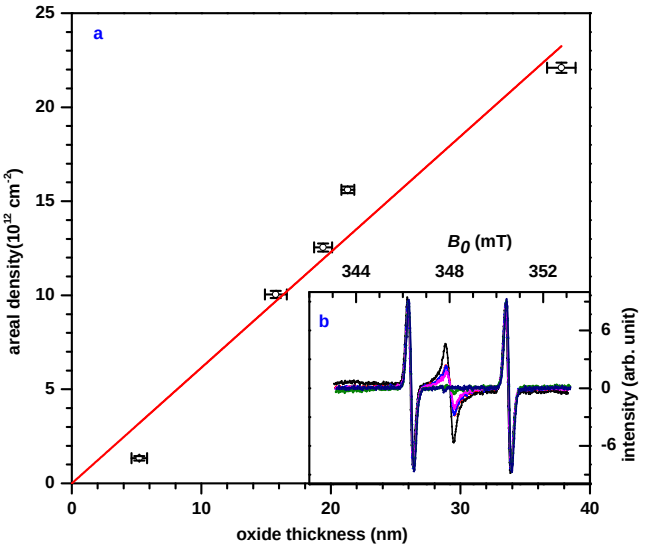

FIG. 3. (a) Plot of the measured E' center area density as a function of the different oxide thicknesses and an offset–free linear fit (red line). The agreement of the measured data and the linear fit indicates that the observed paramagnetic defects created by the Ar^+ plasma are bulk defects. (b) Plots of the EPR spectra measured on SiO_2 samples that have been exposed for different durations to dilute HF. The remaining oxide thickness on each sample was measured by ellipsometry.

oxide) or the plasma etched c-Si surface states (if the oxide was completely removed) could also contribute to the observed signal. In order to explore this question, the depth distribution of the plasma induced paramagnetic states was studied by repetition of the EPR determined density measurement as a function of several oxide thicknesses after the partial removal of the oxide by a wet chemical etch. For this step etch experiment, a dilute HF solution was used. After each HF-etch step, the oxide thickness was measured by ellipsometry and the areal density of the paramagnetic centers was determined by EPR spectroscopy. Figure 3 displays the results of these measurements for both the area concentration as a function of remaining oxide thickness (a) and the raw data given by the EPR spectra of the sample recorded after the individual etch steps (b).

Plot (a) also displays an offset–free linear fit which shows good agreement with the data. This agreement is indicative of a homogeneous distribution of the plasma–generated centers throughout the oxide layer. From the slope of the fit, we obtain a volume density $6.2(3) \times 10^{18}$cm^{-3}. Based on the measurements presented in Fig. 3, we conclude that we have found a method to generate SiO_2 layers with very large densities of paramagnetic E' centers as needed.

A. Thermal and light induced stability of very high E' center density film

In order to study the thermal stability of the large Ar^+ plasma induced E' center densities, we conducted a series of anneal experiments on high density samples that were plasma treated for 5 minutes with the plasma parameters described above. The thermal anneal was then conducted for 20min under ambient conditions at various temperatures between room temperature and 290^{o}C. Using lock–in detected cw EPR, the E' center's area density was then measured as described above and the measured spectra were integrated in order to determine absorption peak areas. The results of these measurements are displayed in Fig. 4(a). The set of spectra illustrates how the plasma generated ensemble of paramagnetic states gradually disappears with increasing anneal temperature. The plot in Fig. 4(b) displays the E' center densities that were derived from the integrated lock–in detected cw EPR measurements as a function of the preceding anneal temperatures. From the difference of the E' densities of the non-annealed sample and this data, one can obtain the density loss as a function of temperature, which is displayed as an Arrhenius plot in Fig. 4(c). The fit of this data with an Arrhenius function reveal an activation energy of $\Delta = 176(1)$meV. The anneal experiments show that plasma induced high E' center densities can be annealed at comparatively low temperature. However, since $\Delta > k_B T_{room}$, room temperature stability of the defects is observed. We note that the observed low activation

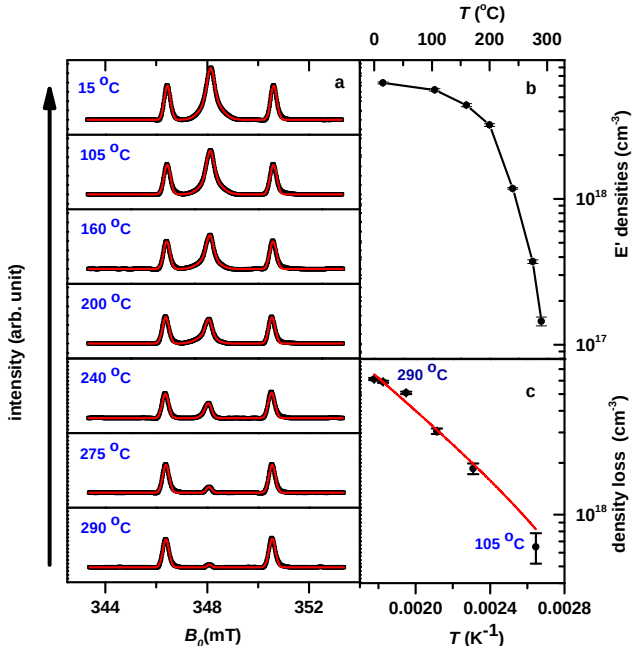

FIG. 4. (a) Integrated lock–in detected cw EPR spectra measured after different annealing temperatures (black lines) and fit of the data with three Gaussian peaks. The density of the E' centers decreases with temperature and at 290°C, it is reduced by an order of magnitude. (b) Plot of the E' center densities obtained from the fit results displayed in (a) as a function of the temperature. (c) Arrhenius plot of the density loss, the difference of the room temperature sample and the annealed samples as a function of the anneal temperature. The fit with an Arrhenius function reveals a resonable agreement and a defect anneal activation energy of 0.176(1)eV.

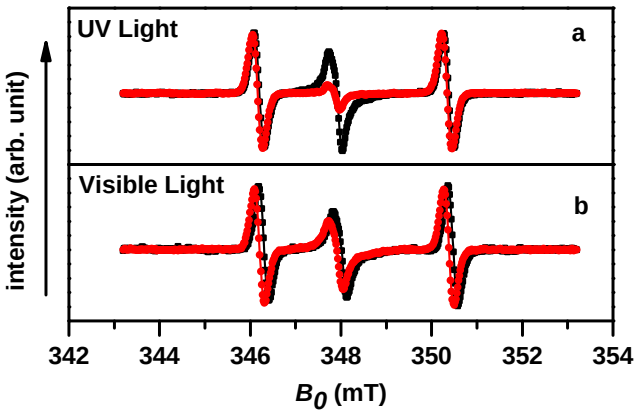

FIG. 5. EPR spectra of high E' center density SiO_2 films measured before (black data) and after (red data) a one hour exposure with UV light (a) and visible light (b). Both photo–bleaching experiments show that the light exposure leads to a reduction of the E' center densities. However, this effect is significantly stronger for UV light exposure.

threshold for E' center recombination appears to be analogous to that of P_b centers at the crystalline silicon to SiO_2 interface. For the latter, Lenahan and Dressendorfer observed a significant reduction of the γ-radiation induced P_b densities (with initial nearest neighbor distances corresponding to those of the E' centers studied here) for similar anneal temperatures ($\approx 250°C$) [33].

In order to further scrutinize the stability of the plasma induced high E' center densities, we have conducted photo–bleaching experiments. We exposed plasma treated but not annealed SiO_2 layers for 60 minutes to two different light sources: (a) a UV source with two strong emission maxima at around 174nm and 254nm, and (b) an incandescent spectral light lamp which emits mostly in the visible wavelength range. Fig. 5 displays two plots, each of which contain two EPR spectra of the plasma etched but otherwise untreated sample and the bleached samples, respectively. The two plots (a) and (b) correspond to the UV bleaching experiment and the visible light experiment, respectively. The data sets show that photo bleaching has a significant effect for both light sources as both post exposure spectra exhibit smaller E' center resonances. However, in comparison to the comparatively minor loss for the visible spectral lamp (b), the exposure by UV light causes a reduction of the E' density by a significantly larger amount. This realization that bleaching can have similar effects as annealing could be significant for the development of low–temperature adjustment of well defined E' center densities.

Finally, we tested the long term stability of the plasma generated high E' center densities at room temperature. Using EPR, we measured repeatedly the density of a plasma treated sample over a time of approximately five weeks. During this time, the sample was kept at ambient conditions and at room temperature. The results of these measurements are displayed in the plot of Fig. 6. Over the course of about month, a clear decline of the E' density to about half of its original value is recognizable. While this is a significant decrease, the resulting half life of the generated E' center densities exceeds by far the expected duration of the single spin experiments for which the high E' center densities are needed.

IV. SPIN RELAXATION DYNAMICS OF E' CENTERS AT HIGH DENSITIES

The application of high density E' center SiO_2 layers for scanning probe based spin readout requires sufficiently long spin relaxation times T_1 and T_2 [9]. The magnetic resonance spectra discussed above give no indication that there is any microscopic difference between E' centers in the high density material reported here compared to previously studied low density materials as resonance line and inhomogeneous line widths are comparable. Consequently, one may hypothesize that the intrinsic relaxation behavior of an individual E' center could be similar or identical in high- and low-density films. However, the decreased average distance between the E' centers at high densities could increase their mutual spin in-

teractions, mostly because of spin–dipolar coupling that becomes significant below 5nm nearest neighbour distances, to a lesser extend because of exchange, since the latter is weak due to the strong localization [14] of the E' center. Spin–spin interaction can directly quench T_2 relaxation times, while T_1 times can be affected by electronic interactions between the localized E' states.

Figures. 7 and 8 show the results of both longitudinal (T_1) and transverse (T_2) spin relaxation times on the high density SiO_2 reported above. For these measurements, we have applied pEPR experiments in a temperature range of $T = 5$K to $T = 70$K. Due to the temperature dependence of equilibrium polarization, spin echo measurements could be conducted on the very small spin ensemble of the thin film samples only up to about 70K. We displayed the data in Figs. 7 and 8 as Arrhenius plots with extrapolations of the experimental data to room temperature and Arrhenius fits, even though, we note that with the overall weak temperature dependencies of the observed spin relaxation dynamics and the given measurement errors, an Arrhenius activation of the observed processes can not be claimed with high significance, nor is it expected in absence of a rigorous theoretical treatment of the E' relaxation dynamics at these very high [E'].

We note that because of the time–dependence of [E'] that was discussed above, the spin–relaxation times were acquired for all measurements within a few hours after the materials preparation. As the measurements for T_1 and T_2 required averaging times on the order of hours, we repeatedly prepared new samples in order to limit the sample age for each measured value to less than 12 hours, a procedure that ensured that [E'] errors due to defect recombination remained low for the reported measurements.

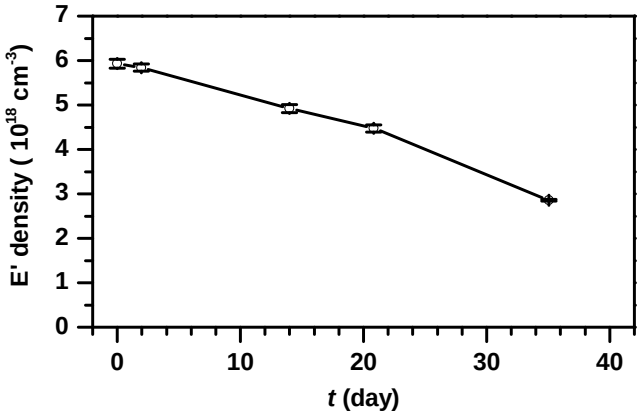

FIG. 6. Plot of EPR measured E' center densities of an SiO_2 layer after plasma treatment over the course of approximately five weeks. A gradual decline of the density is observed. However, the decay is slow enough such that even after about five weeks the absolute volume density still exceeds 10^{18}cm^{-3}.

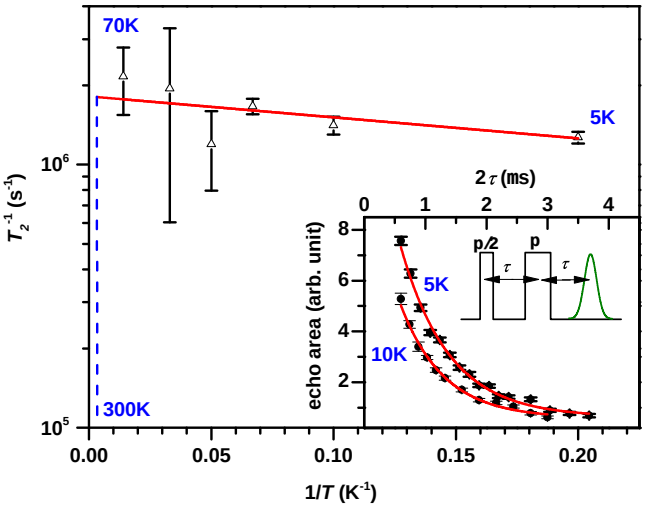

FIG. 7. Plot of the measured transverse E' center spin relaxation rate coefficients T_2^{-1} and their error margins as a function of the inverse temperature. The red line represents a fit with an Arrhenius function. The inset displays a sketch of the Hahn–spin echo sequence that was used to measure T_2 as well as a plot of the measured Hahn–echo intensity as a function of the pulse separation time τ for $T = 5$K and $T = 10$K, with the plots of fits of these data sets with exponential decay functions. Within the given error margins, no temperature dependence of the T_2 relaxation is observed.

A. Transverse spin relaxation

In order to measure T_2 relaxation times, a two pulse Hahn–echo experiment was performed. Figure 7 displays the results of these measurements (the relaxation rate coefficient T_2^{-1}) as a function of the inverse temperature ($1/T$). The data points in this plot were obtained by execution of Hahn–echo decay experiments where a standard Hahn-echo pulse sequence consisting of a $\pi/2 - \pi$ is applied on resonance to the spin ensemble and the integrated intensity of the resulting spin–echo is then measured as a function of the pulse separation time τ. For the examples at low temperature ($T = 5$K, $T = 10$K), the employed pulse sequence as well as the decay data of the Hahn–echo amplitude are displayed in the inset, along with a fit by an exponential decay function which shows agreement with the experimental data.

The measured transverse spin relaxation times of $T_2 \approx 0.5\mu$s showed no significant dependence on temperature. These measurements display significantly shorter T_2 times compared to room temperature values obtained on bulk SiO_2 [23, 34] which suggests that the much higher spin-spin interaction between E' centers due to the higher [E'] causes an increase of the transverse dephasing rate and thus, a shortened T_2. The temperature independence is indicative that phonon-processes do not play a role for T_2.

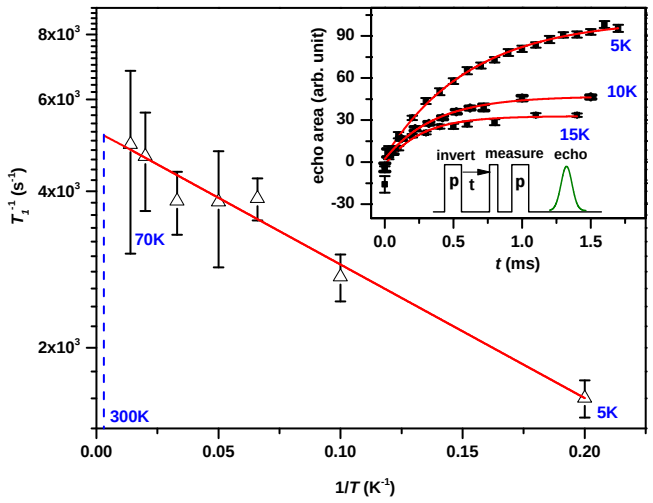

FIG. 8. Plot of the measured longitudinal E' center spin relaxation rate coefficients T_1^{-1} and their error margins as a function of the inverse temperature. The red line represented a fit with an Arrhenius function. The dashed line indicates the room temperature value of T_1 that is extrapolated from the measurements conducted at lower temperatures. The inset displays a sketch of the inversion recovery pulse sequence that was used to measure T_1 as well as a plot of the Hahn-echo intensity as a function of the inversion delay time t for $T = 5$K, $T = 10$K, and $T = 15$K as well as plots of the fit results with exponential recovery functions.

B. Longitudinal spin relaxation

For the measurements of the spin relaxation times T_1, the Hahn-echo pulse sequence used for the T_2 measurements was extended by one pulse such that polarization inversion recovery could be observed. The inset of Fig. 8 displays this pulse scheme which begins with a π-inversion pulse of the spin ensembles equilibrium polarization. After the inversion, a delay time t passes before a Hahn–echo pulse sequence is applied which reveals the residual polarization of the spin ensemble. Measurement of the ensemble polarization as a function of the delay time t will then reveal the dynamics of how the inverted spin polarization right after the inversion pulse gradually relaxes back towards a thermal equilibrium polarization. The inset of Fig. 8 shows plots of the measured polarization as a function of the delay time t for temperatures $T = 5$K, $T = 10$K, and $T = 15$K. The data sets show that for small t, the measured residual polarization is less than 0, representing a negative (inverted) polarization, yet not a fully inverted polarization since not all spins can be flipped due to the amplitude of the inversion pulse. Since the width of the resonance ($\sim$ 2mT) is much larger than the highest driving field strengths that the given experimental setup is able to produce ($\sim$ 1mT), strong dephasing during a π–pulse is expected. The ensemble inversion caused by the pulse is therefore rather an ensemble scrambling that diminishes its polarization. There is also a finite detection dead time of the microwave detector after the inversion recovery sequence is executed, due to which the resonantly induced inversion can only be detected when it has already partially decayed. This reduction of the polarization applies for the detection of both inverted as well as non–inverted ensemble polarization though. For long inversion times t, a positive equilibrium polarization is reestablished.

The experimental data for the inversion recovery transients are well fit by exponential recovery functions and the time constants obtained from these fits represent the measured T_1 values. The main plot of Fig. 8 displays the measured T_1 rate coefficients ($= T_1^{-1}$) as a function of the inverse temperature as well as a plot for an Arrhenius function that has been fit to the experimental data. The extension of this Arrhenius function to $T = 300$K reveals an extrapolated room temperature longitudinal spin relaxation time of $T_1 = 195(5)\mu$s, a value that is in good agreement with T_1 times measured on low density bulk SiO_2 [22, 23], even though this does not validate the applicability of the Arrhenius processes as discussed above. At low temperatures, the longitudinal spin relaxation times are significantly shorter compared to measurements made on low E' center–density SiO_2 [21].

The high T_1 relaxation rates as well as the overall significantly lower temperature dependence of T_1 in high–[E'] SiO_2 compared to low–[E'] SiO_2 [21] and other disordered semiconductor materials that contain silicon dangling bonds (e.g. amorphous silicon [24] or microcrystalline silicon [35]) suggest that at high [E'] and low temperatures, mechanisms other than the pure phonon scattering processes can become dominant. The agreement of T_1 for the highest measured temperature of $T = 70$K and the Arrhenius extrapolation to room temperature with order of magnitude ranges for previously reported values for low–[E'] SiO_2, suggests that longitudinal relaxation at higher temperatures may be governed by direct spin–phonon interaction at high as well as low values of [E']. Systematic studies of the density dependence of dangling bond T_1 relaxation times in SiO_2 have been scarce, both theoretically or experimentally. However, a theoretical study by Murphy [36] pointed out that the spin–lattice relaxation rate of paramagnetic electron states located near ionic tunneling systems that undergo localized motion in SiO_2 can cause the spin–lattice relaxation rate temperature dependence to significantly weaken from the usual quadratic temperature behavior observed without the ionic impurities, towards a linear dependence. To our knowledge, the high–[E'] SiO_2 studied here does not contain any ionic impurities, it is conceivable though that the defect–induced, highly underconstrained character of the continuous random network allows for local motion of the network constituents, including those at which the E' states are located. Furthermore, the E' center can also assume local mobility by undergoing tunnel transitions between different bonding sites [36] causing a weakening of the weak temperature dependence similar to the motion of ionic species. In essence, we conclude that the weak temperature dependence of T_1 is caused by local

motion effect due to rocking, wagging, and stretching of bonds in the vicinity of the E' states or mobility of the E' states.

We notice that silicon dangling bond relaxation processes have been studied to a greater extend in amorphous silicon (a-Si) networks, even though the analogy between amorphous silicon and amorphous SiO_2, is limited, given the abundance of hydrogen in most a-Si materials and the significantly different band structure which caused spin relaxation in a-Si to be affected by electronic mobility effects which do not exist in SiO_2 [37].

Effects of silicon dangling bond densities on the temperature dependencies of spin–lattice relaxation times of silicon dangling bond states in a-Si have been reported before by Stutzmann and Biegelsen [24]. In this work, the dangling bond density was adjusted by thermal annealing, yet in contrast to the study presented here on SiO_2, the anneal caused increases of dangling bond densities due to proton effusion. Similar to our observations reported here, Stutzmann and Biegelsen observed a decrease of the ratio between low temperature and room temperature T_1 values for very high dangling bond densities and similar to the predictions of Murphy [36] for SiO_2, this effect was attributed to spin motion, yet not localized motion but spin diffusion. A study of continuous wave EPR detected silicon dangling bond line width in disordered silicon by Nickel and Schiff [38] also revealed a weak and, therefore, an unconventional temperature dependence for samples with high ($\approx 10^{18}\text{cm}^{-3}$) dangling bond densities.

While we stress that it is not clear to what extent the spin–lattice relaxation dynamics of silicon dangling bonds in disordered silicon is comparable to disordered SiO_2, we again conclude that the hypothesis that local motion effects caused by the underconstrained network, combined with increased spin–spin interactions due to the decreased average E' center distances, is consistent with the observed different longitudinal spin–relaxation behaviors at high and low values of [E'].

For the assessment of whether or not the E' center spin–relaxation times of high-[E'] SiO_2 presented here render the E' center suitable for their application as probe spins within for SSTFM described by Payne et al. [9], we reiterate that since spin–detection using this concept is based on the discrimination of random telegraph noise powers caused by a change of the noise power spectra under magnetic resonance, the intrinsic spin–flip rate of a probe spin is limited by the longitudinal spin relaxation time T_1 in absence of magnetic resonance, while the spin–flip rate is governed by the resonant driving field B_1 on-resonance. Thus, next to the geometric requirements of the probe spins discussed above (high localization, presence of a single center at the probe tip), the suitability of a paramagnetic state as probe spin requires that $T_1 > \gamma B1$ with γ being the electrons gyromagnetic ratio. The magnitude of T_2 poses no limitation for the readout concept since spin–phase loss has no effect on the projective measurement of a coherent spin–pair state onto an spin–pair eigenstate. For technologically straight forwardly achievable driving fields in a scanning probe setup of $B_1 \approx 0.1\mu\text{T}$, this requires $T_1 >\sim 0.1\text{ms}$. We therefore conclude that E' centers, even at the highest densities reported here and room temperature, posses adequate spin relaxation properties as spin probes for the SSTFM based single spin–readout proposed by Payne et al [9].

V. SUMMARY AND CONCLUSIONS

The suitability of the spin–relaxation dynamics of E' centers within 60nm thin amorphous SiO_2 layers for the application of E' centers as probe spins for SSTFM has been studied. The experiments have shown that for SiO_2, with Ar^+ ion plasma induced optically and chemically stable densities of $[\text{E}'] > 5 \times 10^{18}\text{cm}^{-3}$, the transverse spin–relaxation time displays an average $T_2 = 552(15)\text{ns}$, with no significant dependence on the temperature between $T = 5\text{K}$ and $T = 70\text{K}$. Within the same temperature range, the spin-lattice relaxation time (T_1) exhibits a slightly stronger, yet compared to low–[E'] SiO_2 nevertheless weak temperature dependence. By extrapolation of this weak temperature dependence of T_1 to room temperature through an Arrhenius function, a room temperature value of $T_1 \approx 195(5)\mu\text{s}$ is found, in good agreement with literature values for low–[E'] SiO_2. At $T = 5\text{K}$, $T_1 = 625(51)\mu\text{s}$, which is significantly shorter than the low–[E'] $T_1 \approx 1s$[21].

We conclude that the observed T_1 and T_2 times as well as the long–term stability of the E' center at high density makes this defect an excellent candidate for applications as probe–spin in the spin–selection rule based force–detected SSTFM scheme proposed by Payne et al. [9]. SSTFM using E' centers may allow for suitable readout approaches for silicon based spin quantum information or spintronics applications, even at room temperature where for technologically achievable spin resonant driving fields, T_1 is required to exceed $100\mu\text{s}$.

ACKNOWLEDGMENTS

We acknowledge the support by the NSF Materials Research Science and Engineering Center (MRSEC) at the University of Utah (#DMR11-21252, in support of K. A.), the NSF Major Research Instrumentation program (#0959328 in support of instrumentation acquisition as well as K. A., C. W., and C. B), the Army Research Office (#W911NF-10-1-0315 in support of A. P.), and the NSF CAREER program (#0953225 in support of D. P. W.).

[1] J Wrachtrup, C Von Borczyskowski, J Bernard, M Orritt, and R Brown, "Optical detection of magnetic resonance in a single molecule," (1993).

[2] Daniel Rugar, R Budakian, HJ Mamin, and BW Chui, "Single spin detection by magnetic resonance force microscopy," Nature **430**, 329–332 (2004).

[3] J. R. Petta *et al.*, "Coherent manipulation of coupled electron spins in semiconductor quantum dots," Science **309**, 2180–2184 (2005).

[4] Andrea Morello *et al.*, "Single-shot readout of an electron spin in silicon," Nature **467**, 687–691 (2010).

[5] M. Bode, M. Heide, K. Von Bergmann, P. Ferriani, S. Heinze, G. Bihlmayer, A. Kubetzka, O. Pietzsch, S. Blügel, and R. Wiesendanger, "Chiral magnetic order at surfaces driven by inversion asymmetry," Nature **447**, 190–193 (2007).

[6] H. J. Mamin *et al.*, "Nanoscale nuclear magnetic resonance with a nitrogen-vacancy spin sensor," Science **339**, 557–560 (2013).

[7] Uwe Kaiser, Alexander Schwarz, and Roland Wiesendanger, "Magnetic exchange force microscopy with atomic resolution," Nature **446**, 522–525 (2007).

[8] Roland Wiesendanger, "Spin mapping at the nanoscale and atomic scale," Reviews of Modern Physics **81**, 1495 (2009).

[9] A. Payne, K. Ambal, C. Boehme, and C.C. Williams, "Atomic-resolution single-spin magnetic resonance detection concept based on tunneling force microscopy," Phys. Rev. B **91**, 195433 (2015).

[10] C. Boehme and K. Lips, "Spin-dependent recombination - an electronic readout mechanism for solid state quantum computers," Phys. Stat. Solidi B **233**, 427–435 (2002).

[11] A. R. Stegner, "Electrical detection of coherent ^{31}P spin quantum states," Nature Phys. **2**, 835–838 (2006).

[12] S.-Y. Paik, S.-Y. Lee, W. J. Baker, D. R. McCamey, and C. Boehme, "T_1 and T_2 spin relaxation time limitations of phosphorous donor electrons near crystalline silicon to silicon dioxide interface defects," Phys. Rev. B **81**, 075214 (2010).

[13] T. W. Herring, S.-Y. Lee, D. R. McCamey, P. C. Taylor, K. Lips, J. Hu, F. Zhu, A. Madan, and C. Boehme, "Experimental discrimination of geminate and non-geminate recombination in $a-Si:H$," Phys. Rev. B **79**, 195205 (2009).

[14] P. M. Lenahan and J. F. Conley, "What can electron paramagnetic resonance tell us about the Si/SiO_2 interface system?" J. Vac. Sci. Technol. B **16**, 2134–2153 (1998).

[15] P.M. Lenahan and J.J. Mele, "E′ centers and leakage currents in the gate oxides of metal oxide silicon devices," J. Vac. Sci. Technol. B **18**, 2169–2173 (2000).

[16] R. A. Weeks, R. and C. M. Nelson, "Trapped electrons in irradiated quartz and silica: II, electron spin resonance," J. Am. Ceram. Soc. **43**, 399–404 (1960).

[17] R.A. Weeks, R.H. Magruder, and Andre Stesmans, "Review of some experiments in the 50 year saga of the E′ center and suggestions for future research," J. Non-Cryst. Solids **354**, 208 – 216 (2008).

[18] N. M. Atherton, *Principles of Electron Spin Resonance* (Ellis Horwood PTR Prentice Hall, Chichester, 1993).

[19] A. Schweiger and G. Jeschke, *Principles of Pulse Electron Paramagnetic Resonance* (Oxford University Press, Oxford, 2001) pp. –.

[20] J. G. Castle, D. W. Feldman, P. G. Klemens, and R. A. Weeks, "Electron spin-lattice relaxation at defect sites; E′ centers in synthetic quartz at 3 kilo-oersteds," Phys. Rev. **130**, 577–588 (1963).

[21] J.G. Castle and D.W. Feldman, "Temperature dependence of paramagnetic relaxation at point defects in vitreous silica," J. Appl. Phys. **36**, 124–128 (1965).

[22] S.S. Eaton and G.R. Eaton, "Irradiated fused-quartz standard sample for time-domain EPR," J. Magn. Reson. Ser. A **102**, 354–356 (1993).

[23] B.T. Ghim, S.S. Eaton, G.R. Eaton, R.W. Quine, GA Rinard, and S. Pfenninger, "Magnetic field and frequency dependence of electron spin relaxation times of the E′ center in irradiated vitreous silica," Journal of Magnetic Resonance, Series A **115**, 230–235 (1995).

[24] M. Stutzmann and D. K. Biegelsen, "Electron-spin-lattice relaxation in amorphous silicon and germanium," Phys. Rev. B **28**, 6256–6261 (1983).

[25] C. Malten, J. Mueller, and F. Finger, "Pulsed EPR studies on doped microcrystalline silicon," Phys. Stat. Solidi B **201**, R15–R16 (1997).

[26] C. Böhme, *Dynamics of spin-dependent charge carrier recombination* (Cuvillier, Göttingen, 2003).

[27] J. C. Phillips and M.F. Thorpe, "Constraint theory, vector percolation and glass formation," Solid State Commun. **53**, 699 (1985).

[28] G. Lucovsky, Y. Wu, H. Niimi, V. Misra, and J.C. Phillips, "Bonding constraints and defect formation at interfaces between crystalline silicon and advanced single layer and composite gate dielectrics," Appl. Phys. Lett. **74**, 2005–2007 (1999).

[29] K. Yokogawa, Y. Yajima, T. Mizutani, S. Nishimatsu, and K. Suzuki, "Positive charges and E′ centers formed by vacuum ultraviolet radiation in SiO_2 grown on Si," Jpn. J. Apl. Phys. **29**, 2265–2268 (1990).

[30] M. E. Zvanut, R. E. Stahlbush, and W. E. Carlos, "Radiation induced E′ centers in H_2 annealed oxide films," Appl. Phys. Lett **60**, 2989–2991 (1992).

[31] Y. Ishikawa, M. Okigawa, S. Samukawa, and S. Yamasaki, "Reduction of plasma-induced damage in SiO_2 films during pulse-time-modulated plasma irradiation," J Vac. Sci. Technol. B **23**, 389 (2005).

[32] Y. Ichihashi, Y. Ishikawa, Y. Kato, R. Shimizu, M. Okigawa, and S. Samukawa, "Effects of thermal annealing for restoration of UV irradiation damage during plasma etching processes," Jpn. J. Apl. Phys. **45**, 8370 (2006).

[33] P. M. Lenahan and P. V. Dressendorfer, "An electron spin resonance study of radiation-induced electrically active paramagnetic centers at the Si/SiO_2 interface," J. Appl. Phys. **54**, 1457 (1983).

[34] M. Ikeya, H. Kohno, S. Toyoda, and Y. Mizuta, "Spin-spin relaxation time of E′ center in neutron radiated quartz," Jpn. J. Appl. Phys. **31**, L1539 (1992).

[35] F. Finger, J. Müller, C. Malten, and H. Wagner, "Electronic states in hydrogenated microcrystalline silicon," Phil. Mag. B **77**, 805–830 (1998).

[36] J Murphy, "Spin-lattice relaxation due to local vibrations with temperature-independent amplitudes," Phys. Rev.

145, 241 (1966).

[37] Nicholas J Harmon and Michael E Flattè, "Spin relaxation in materials lacking coherent charge transport," Phys. Rev. B **90**, 115203 (2014).

[38] N. H. Nickel and E. A. Schiff, "Direct observation of dangling bond motion in disordered silicon," Phys. Rev. B **58**, 1114 (1998).